Kondo-Majorana coupling in Double Quantum Dots.

by

Jesús David Cifuentes Pardo

Advisor: Luis Gregorio Dias da Silva

MASTER OF SCIENCE

in

Instituto de Física

(Condensed Matter Physics)

UNIVERSIDADE DE SÃO PAULO

(R. do Matão, 1371 - Butantã, São Paulo)

January 23, 2019

Chapter 1

Abstract

In the last decades the interest in the “search of Majorana fermions” in condensed matter systems [1] has increased due to their potential applications in quantum computing. As recently as 2012, experimental works reporting the detection of such quasiparticles [2, 3]. Later works [4, 5, 6, 7], including a recent paper published by the advisor of this dissertation and collaborators [8], set out to explore the interplay of such Majorana zero-modes with strongly interacting systems such as semiconductor quantum dots, which can be readily integrated in the device. This research project aims to expand this idea using the numerical renormalization group to study the model of a double quantum dot coupled to metallic leads and to a topological superconductor supporting edge Majorana zero modes. This simple model allows the manipulation of the majorana modes bringing possible applications to braiding procedures . In addition, we will study the interplay of Kondo correlations, exchange interactions and Majorana physics.

Chapter 2

Table of Contents

Chapter 3

Preliminaries

We will start with a description of transport processes in QDs which will lead us to talk about the Anderson model. Then we will take a look to the Kondo effect and, in particular, to its consequences in quantum dots.

3.1 Transport in Quantum Dots (QDs)

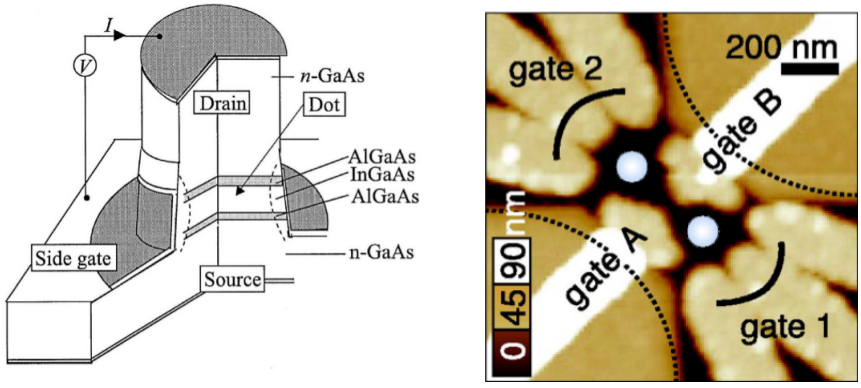

(a) (b)

Figure 3.1: a) Vertical quantum dot. b)Atomic force microscopy picture of two coupled lateral QDs (bright central circles). Gates 1 and 2 act as drain and source voltage. A negative voltage is applied at gates A,B to allow the formation of the droplets inside the free space in the 2D electron gas.
Source: *[9]*

Quantum mechanical effects are visible when the system size is of the order of the de Broglie wavelength [10, (1.1)]

$$\lambda_f = \frac{h}{\sqrt{3 m_{\text{eff}} k_B T}}$$

where m_{eff} is the electron effective mass in the crystal. Since m_{eff} can be much smaller than the free electron mass in some semiconducting materials, size quantization effects can be observed at system of sizes $\sim$ 100nm [11, 2.1]. A 0D quantum system is a device confined in the three

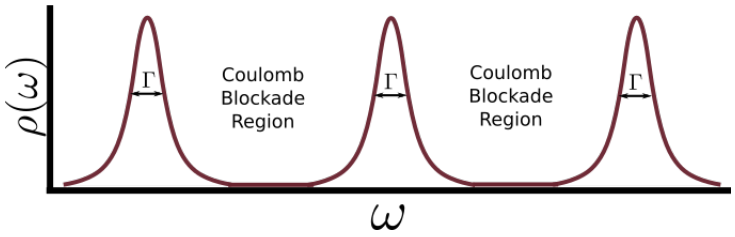

Figure 3.2: Pictorial representation of the Density of States of a QD. The gate potential V_G can be tuned to change the fermi energy of the dot.
Source: *By the author*

spacial dimensions up to this length-scale. This type of devices receive the name of quantum dots (QD).

QDs can be manufactured with several methods, forms and orientations [10]. Note *Methods and forms* According to their orientation with respect to the based 2D-plane two main types of QDs can be distinguished : Vertical (Figure 3.1a) and lateral (Figure 3.1b) QDs. Both types of quantum dots have 3-main gates. Two of them are the Drain V_D and source V_S gate voltages used to control the current through the QD. The third one is the gate voltage V_G which controls the electron confinement inside the QD by tuning the the energy levels .

Ideally, the energy spectrum of a QD is a discrete set of energy levels resembling the spectrum of an atom. However, when the QD is connected to metallic leads these energy levels hybridized with respect to a hybridization parameter Γ which depends on the voltage connecting the lead with the dots V as

$$\Gamma \propto \pi \|V\|^2 \tag{3.1}$$

in a flat band. A representation of this fact can be found in Figure 3.2. Ideally, $\Gamma \ll \Delta E$ such that the energy levels do not overlap each other. In addition the gate voltage allows us to tune the energy levels of the QD.

It is possible to execute transport measurements through a QD by attaching it to two leads, source and drain (See 3.3a) . Each lead will have a characteristic gate voltage V_S (Left lead) and V_D (Right lead). An electron can pass from the source to the drain if there is an energy level in the middle of the two voltages, just as in 3.3a. If this condition is not satisfied, the dot enters into a coulomb blockade region without electron transport between both leads as can be observed in 3.4b. Inside the coulomb blockade regions the number of electrons is constant. When increasing V_G a single electron enters into the dot each time. Since all of these effects can be controlled by a tuning the gate voltage, the system described is indeed a single electron transistor (SET).

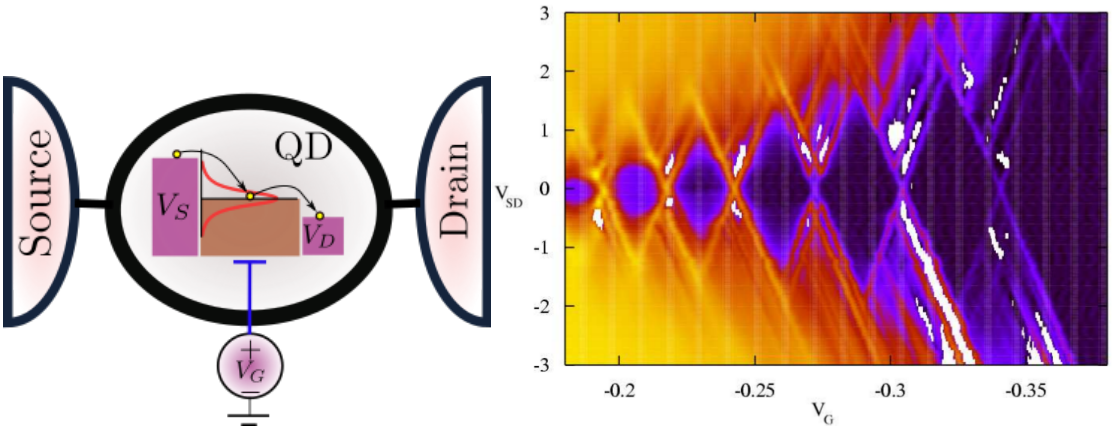

(a) (b)

Figure 3.3: a) Representation of transport through QD. The red curve represents the hybridized energy level. The gate voltage tunes this level. In the case represented, the energy level is in the middle of the drain and source voltages allowing transport between the leads. Charging diagram of a quantum dot. b) Plot of the conductance vs the gate voltage V_G and the source-drain voltage $(V_{SD} = V_S - V_D)$

Source: *a) By the Author , b) [11]*

3.2 The Anderson Model

The Anderson model [12] was originally created to study the physics of impurities. This includes magnetic impurities in metals that are responsible for the Kondo effect as well as artificial impurities like QDs.

In this thesis we will mainly discuss to regimes. here are two regimes that will be particularly important in this thesis. They depend on whether Coulomb repulsion is important or not. These are

- **Non-interacting systems:** Coulomb repulsion is not relevant . In this case, spin-$\uparrow$ and spin-$\downarrow$ channels are independent which simplifies many of the procedures. The method used to describe this systems is ballistic transport.

- **Interacting systems:** The coulomb repulsion is relevant. The repulsion factor will be defined by the factor U. In this case, the spin-$\uparrow$ and spin-$\downarrow$ channels are not independent since the coulomb repulsion limits the number of particles inside each dot. We will use the Numerical Renormalization Group to treat this kind of systems.

Using the Hunds rules we know that the energy levels inside the dot should be filled from lower to higher energies with two electrons with different spin at each state. Each pair of

electrons will interact magnetically and electrically. In addition, there is and energy associated to each electron and a Zeeman splitting factor in case a $\hat{z}$-directed magnetic field B is placed. Considering these interactions we can obtain a very general expression in second quantization for the QD Hamiltonian of the form [11, (3.2)]

$$H_d = \sum_{i\sigma} \varepsilon_{di} d^\dagger_{i\sigma} d_{i\sigma} + \sum_i U_i \hat{n}_{i\uparrow}\hat{n}_{i\downarrow} + \sum_{\sigma\sigma', i\neq j} U_{ij}\hat{n}_{i\sigma}\hat{n}_{j\sigma'} - \mu_B g B \sum_i S^z_i + J\sum_{i\neq j} \mathbf{S}_i \cdot \mathbf{S}_j.$$

Where $\sigma \in \{\uparrow,\downarrow\}$, $d^\dagger_{i\sigma}\,(d_{i\sigma})$ is the dot creation(annihilation) operator,$\hat{n}_{i\sigma} := d^\dagger_{i\sigma} d_{i\sigma}$ is the particle number, $\mathbf{S}_i$ is the spin-vector, ε_{di} is the energy of the i^{th}-level in the dot, U_i is the coulomb repulsion between electrons in the same energy level i, U_{ij} is the coulomb interaction between electrons in different levels (And therefore smaller than U_i), B is an applied magnetic field in the $\hat{z}$-direction and J is the term representing the Zeeman splitting.

At low temperatures, the main interactions only with the level closest to the Fermi energy. This allows us to make the single-level approximation, neglecting the other energy levels. This assumption reduces the complexity of the dot Hamiltonian to

$$H_d = \sum_\sigma \varepsilon_d d^\dagger_\sigma d_\sigma + U\hat{n}_\uparrow\hat{n}_\downarrow - \mu_B g B S^z. \tag{3.2}$$

The lead Hamiltonian is decomposed in two parts. The energy of the electrons inside the leads H_{lead} and the interaction between the leads and the quantum dot H_{int}. These Hamiltonians take the form

$$\begin{aligned} H_{lead} &= \sum_{\mathbf{k}\sigma l} \varepsilon_{\mathbf{k}l} c^\dagger_{\mathbf{k}\sigma l} c_{\mathbf{k}\sigma l} \\ H_{int} &= \sum_{\mathbf{k}\sigma l} V_{\mathbf{k}l} c^\dagger_{\mathbf{k}\sigma l} d_\sigma + V^*_{\mathbf{k}l} d^\dagger_\sigma c_{\mathbf{k}\sigma l}, \end{aligned}$$

where $\mathbf{k}$ represents the possible crystal momentums in the leads, $l \in \{S,D\}$, $c^\dagger_{\mathbf{k}\sigma l}(c_{\mathbf{k}\sigma l})$ creates(annihilates) an electron with momentum $\mathbf{k}$ and spin σ in the lead l, $\varepsilon_{\mathbf{k}l}$ is the energy of the electron in the leads and $V_{\mathbf{k}l}$ is a hopping exchange term between the leads and the QD.

In conclusion the sum of these three interactions is receives the name of Anderson Model.

$$\begin{aligned} H &= H_d + H_{lead} + H_{int} \\ &= \sum_\sigma \varepsilon_d d^\dagger_\sigma d_\sigma + U\hat{n}_\uparrow\hat{n}_\downarrow - \mu_B g B S^z + \sum_{\mathbf{k}\sigma l} \varepsilon_{\mathbf{k}l} c^\dagger_{\mathbf{k}\sigma l} c_{\mathbf{k}\sigma l} + \sum_{\mathbf{k}\sigma l} V_{\mathbf{k}l} c^\dagger_{k\sigma l} d_\sigma + V^*_{\mathbf{k}l} d^\dagger_\sigma c_{\mathbf{k}\sigma l}. \end{aligned} \tag{3.3}$$

For this project, we will make two extra changes to the Anderson model. Using the anti-commutation properties of the fermion operators

$$\{d_\sigma^\dagger, d_{\sigma'}\} = \delta_{\sigma\sigma'} \ , \ \left\{d_\sigma^\dagger, d_{\sigma'}^\dagger\right\} = \{d_\sigma, d_{\sigma'}\} = 0$$

we get

$$\begin{aligned}\left(d_\uparrow^\dagger d_\uparrow + d_\downarrow^\dagger d_\downarrow - 1\right)^2 &= \sum_\sigma \left(d_\sigma^\dagger d_\sigma\right)^2 - 2\sum_\sigma d_\sigma^\dagger d_\sigma + 2d_\uparrow^\dagger d_\uparrow d_\downarrow^\dagger d_\downarrow - 1 \\ &= 2d_\uparrow^\dagger d_\uparrow d_\downarrow^\dagger d_\downarrow - \sum_\sigma d_\sigma^\dagger d_\sigma - 1.\end{aligned}$$

Replacing this in (3.2) we obtain a nice spin-symmetric form of the dot hamiltonian

$$\left(\varepsilon_d + \frac{U}{2}\right) d_\sigma^\dagger d_\sigma + \frac{U}{2}(d_\sigma^\dagger d_\sigma - 1)^2 - \mu_B g B S^z. \tag{3.4}$$

In addition, it is possible to do a linear transform to the lead opperators

$$\frac{1}{\sqrt{V_S^2 + V_R^2}} \begin{bmatrix} V_S & V_R \\ -V_R & V_S \end{bmatrix} \begin{bmatrix} c_{\mathbf{k}\sigma S} \\ c_{\mathbf{k}\sigma D} \end{bmatrix} = \begin{bmatrix} c_{\mathbf{k}\sigma +} \\ c_{\mathbf{k}\sigma -} \end{bmatrix} \tag{3.5}$$

After the transformation the operator will be decoupled from the dot hamiltonian $c_{\mathbf{k}\sigma -}$. This implies that we can suppose that the **dot is coupled wit just one lead**. During the rest of the thesis we will mantain this convention.

3.3 The Kondo Effect

Note *Here goes a review about the Kondo Effect. I am still trying to figure out how it section will look like. For now Im just leaving some ideas and plots.*

The resistivity of a metal is regulated by different scattering parameters including lattice vibrations $\rho_{phonon} \sim T^5$, electron-electron scattering $\sim T^2$ and the scattering between electrons and static impurities which is temperature independent. The form of these contribution implies that the resistivity decays uniformly with a decrease in temperature. Nevertheless, in the early 30s groundbreaking experiments revealed the observation of a resistance minimum in some metals at temperatures lower than $10K$ (See 3.4a). This phenomenon intrigued the scientific community for following decades until the year 1964 when the physicist Jun Kondo made a major contribution to the field. Kondo attributed this phenomenon spin-scattering of the electrons with a small concentration of magnetic impurities in the metal.

$$H_K = H_l + 2J\hat{\mathbf{S}} \cdot \hat{\mathbf{s}}_0 \tag{3.6}$$

where $\hat{\mathbf{S}}$ and $\hat{\mathbf{s}}_0$ denot the impurity and the conduction spin operators. Kondo computed the resistivity using perturbation theory of H_K over the parameter J, obtaining that the second order correction diverges logaritmically for temperatures $T < T$:

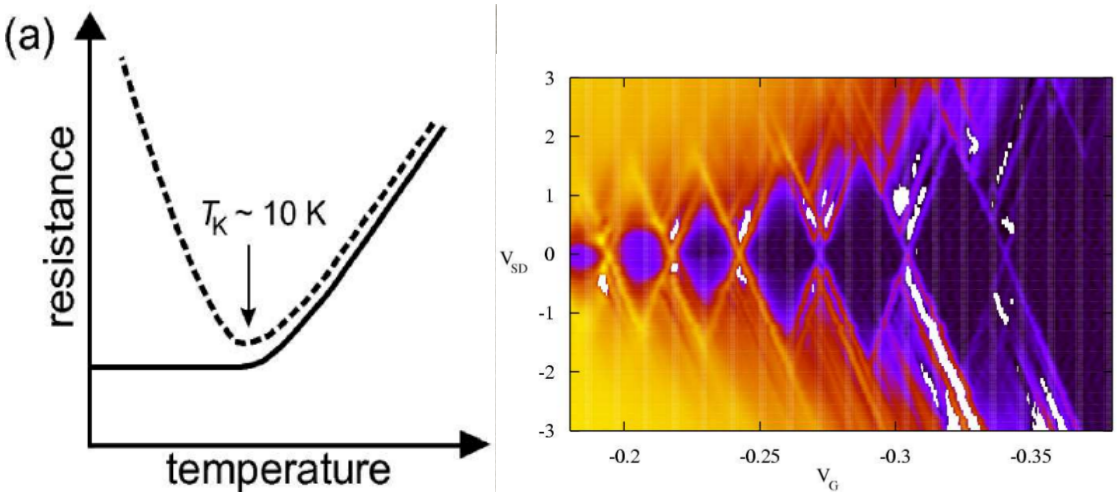

(a) (b)

Figure 3.4: a) Representation of transport through QD. The red curve represents the hybridized energy level. The gate voltage tunes this level. In the case represented, the energy level is in the middle of the drain and source voltages allowing transport between the leads. Charging diagram of a quantum dot. b) Plot of the conductance vs the gate voltage V_G and the source-drain voltage $(V_{SD} = V_S - V_D)$

Source: *a) [13] , b) [11]*

Kondo explained that the conducting electrons in the metal scattered with the electrons in the impurity due to the spin interaction.

[14]

The resistivity of materials is known to decay linearly with

In low temperature metals the resistivity decays uniformly with the temperature due to the absence of scattering electrons at lower energies. However, in the early 30s the physicist where intrigued by the observation of a resistance minimum in some metals at temperatures near to $10K$ [11]. The effect was studied by the material physicist Kondo who attributed this phenomenon to a small concentration of magnetic impurities in the metal [14]. Kondo explained that the conducting electrons in the metal scattered with the electrons in the impurity due to the spin interaction.

The resistivity of a metal is normally regulated by different scattering parameters including lattice vibrations $\rho_{phonon} \sim T^5$

Using perturbation theory is possible to explain how this spin flip produces a temperature dependent effect which introduces an additional logarithmic term to the resistivity of the form

$$\rho_{Kondo}(T) \propto \ln\left(\frac{T_{kondo}}{T}\right), \tag{3.7}$$

$$\rho(T) = \rho_0 + aT^2 + c_m \ln \frac{\mu}{T} + bT^5, \tag{3.8}$$

which occurs due to the spin-flip between the particles in the impurity and in the reservoir. The entire resistivity including and

We can seen that under the scale of temperature defined by T_k the Kondo effect dominates over all other interactions. However, there is a fundamental problem in the Kondo model. For temperatures much smaller than T_K the resistivity diverges. This problem is solved by applying a re-normalization group approach to treat the strong correlations appearing at low temperatures. In the Kondo problem a logarithmic discretization is used. The numerical procedure receives the name of Numerical renormalization Group (NRG).

3.3.1 Kondo Effect in QDs

The problem of magnetic impurities in metals can be treated using the Anderson model in a similar form as the transport in quantum dots. Hence, it is not a surprise that Kondo Effect could also occur in QDs. When an odd number of electrons is in the QD the last level bellow the Fermi energy is half-occupied and hence the dot is magnetized. The unlocalized electrons in the reservoirs then interact with this localized electron . Spin-flip can occur as in the case of magnetic impurities in metals. At low temperatures, this magnetic interaction gives rise to strong quantum correlations that favor the formation of a singlet state between the localized electron and the electrons in the leads. As a result, the zero-bias density of states is increased producing a zero-bias conductance peak.

Note that the physical implications of the Kondo effect between the case of magnetic impurities in metals and transport through QD are different. The reason for this is difference in the dimension in both processes . While the scattering at 3D systems against magnetic impurities should produce a drop in the conductivity at low temperatures, the scattering in 0D systems enhances the conductivity of the QD due to the few scattering directions. This implies that the Kondo Effect in QDs acts in the opposite way as in the impurity case.

Chapter 4

Theory and Methods

4.1 Ballistic transport

The Green function G of a Hamiltonian H is the operator that satisfies the homogenous equation

$$\left(i\hbar\frac{\partial}{\partial t} - H\right) G\left(t-t'\right) = \delta(t-t'). \tag{4.1}$$

This type of differential equations are solved taking the Fourier transform

$$G_H(\omega) = \int_{-\infty}^{\infty} G(t-t')e^{i\omega(t-t')/\hbar}\delta(t-t') \tag{4.2}$$

In this new space the solution of the equation is

$$(\omega + is - H)G_\omega(\omega) = I.$$

The term $+is$ in the previous hamiltonian is part of a mathematical trick quite common in this theory. During the whole procedure, the Green function acts on the complex field. But when we need to obtain a physical interpretation we will take the limit $s \to 0$ to obtain the result for real energies. The next step is to decompose $G_H(\omega)$ in the eigenbase of the Hamiltonian $\{|\alpha\rangle\}$ by

$$G_{\alpha,\alpha'}(\omega) = \langle\alpha|G_H(\omega)|\alpha'\rangle = \frac{\delta_{\alpha\alpha'}}{\omega - is - \varepsilon_\alpha} = \frac{\delta_{\alpha\alpha'}(\omega + is - \varepsilon_\alpha)}{(\omega-\varepsilon_\alpha)^2 + s^2}. \tag{4.3}$$

From the famous formula

$$\lim_{s\to 0}\frac{s}{(\omega-\varepsilon_\alpha)^2+s^2} = \pi\delta(\omega-\varepsilon_\alpha) \tag{4.4}$$

we obtain

$$Im[G_{\alpha,\alpha'}(\omega)] = \pi\delta(\omega-\varepsilon_\alpha)\delta_{\alpha,\alpha'}. \tag{4.5}$$

Note that the sum of $Im[G_{\alpha,\alpha}(\omega)]$ over all the eigenstates of H is simply the π times the Density of States:

$$\rho(\omega) = -\frac{1}{\pi} Im\left[G_{\alpha,\alpha}(\omega)^\dagger\right]. \tag{4.6}$$

An extended definition of the Green function can be given in terms of fermionic operators in second quantization. The time-green function for two fermionic operators A and B is

$$G_{A,B}(t-t') = \mathscr{T}[\{A(t),B(t')\}]. \tag{4.7}$$

Here, causality is important, which is the reason why we use the time-order operator $\mathscr{T}$. Again, it is possible to define the green-functions in the energy space applying a Fourier transform. The evolution of these Green functions will be determined by the Schrodinger equation. At the end, the result will be

The equation above receives the name of transport equation. This will be our leading method to compute the green functions of the system. In addition we can define the Density of States associated to an operator A to be

$$\rho_{A,A^\dagger} = -\frac{1}{\pi} Im\left[G_{A,A^\dagger}(\omega)\right]. \tag{4.8}$$

This density of states contains important physical information related to operator A. In our case, operator $A^\dagger$ will be related to the creation operator of a quantum dot $d^\dagger$. Our mean purpose will be to compute the density of states of a quantum dot $\rho_{d,d^\dagger}$. This that allows us to obtain other transport

4.1.1 Using graph theory to solve the transport equations

Solving the transport equations involves dealing with a set of linear equations where all the possible variables including ω , and the Hamiltonian parameters are assumed to be constant. This can be done by Gauss-Jordan elimination, noting that after each elimination process we need to carry on the account in terms of these variables. The solution will be a polynomial fraction with the variable given by these parameters. When the number of operators in the Hamiltonian increases the number of terms in the polynomial grows-up exponentially. This reveals the importance of exploring new methods that could simplify the solution.

The method presented here uses graph theory algorithms that provide a shortcut to Gauss-Jordan elimination [15]. To probe this method we solve here the transport equations for a non-interacting $(U = 0)$ DQD connected to one lead. According to the Anderson model the Hamiltonian for this system looks like

$$H = t_{dots} d_1^\dagger d_2 + t_{dots}^* d_2^\dagger d_1 + \sum_{i=1}^{2} \varepsilon_{di} d_i^\dagger d_i + \sum_k \left(V_i d_i^\dagger c_{\mathbf{k}} + V_i^* c_{\mathbf{k}}^\dagger d_i\right) + \varepsilon_{\mathbf{k}} c_{\mathbf{k}}^\dagger c_{\mathbf{k}}. \tag{4.9}$$

Since the system is non-interacting we ignore the spin-degeneracy of this Hamiltonian. The only new parameter here is the term t_{dots}, which represents the tunneling between both quantum dots. Using equation (**??**) with $B = d_1^\dagger$ and A shifting among other operators we compute the

following transport equations

$$(\omega-\varepsilon_1)\,G_{d_1,d_1^\dagger}(\omega)=1+t_{dots}G_{d_2,d_1^\dagger}(\omega)+V_1^*\sum_{\mathbf{k}}G_{c_\mathbf{k},d_1^\dagger}(\omega) \tag{4.10}$$

$$(\omega-\varepsilon_\mathbf{k})\,G_{c_\mathbf{k},d_1^\dagger}(\omega)=V_1G_{d_1,d_1^\dagger}(\omega)+V_2G_{d_2,d_1^\dagger}(\omega) \tag{4.11}$$

$$(\omega-\varepsilon_2)\,G_{d_2,d_1^\dagger}(\omega)=t_{dots}G_{d_1,d_1^\dagger}(\omega)+V_2^*\sum_{\mathbf{k}}G_{c_\mathbf{k},d_1^\dagger}(\omega) \tag{4.12}$$

This system is already closed which means that we don't need any other equation to find the solution. The matrix form takes the form

$$\begin{bmatrix}\omega-\varepsilon_2 & -V_2 & -t_{dots}\\ -V_2^* & \omega-\varepsilon_k & -V_1\\ -t_{dots}^* & -V_1^* & \omega-\varepsilon_1\end{bmatrix}\begin{bmatrix}G_{c_\mathbf{k},d_1^\dagger}(\omega)\\ G_{d_2,d_1^\dagger}(\omega)\\ G_{d_1,d_1^\dagger}(\omega)\end{bmatrix}=\begin{bmatrix}0\\0\\1\end{bmatrix} \tag{4.13}$$

By convenience we changed the order of the rows in the matrix and we removed the sum over k ($\sum_k$) to simplify the terms in the matrix. We will intert these terms back in the equations at the end of the procedure.

Although this matrix is not Laplacian, the procedure in [15] can still be applied with the downside of loosing part of the speed-up of the algorithm. We still preserve some of the advantages using graphs, such as the possibility of taking minimal cuttings and the relation between Gauss-Jordan elimination and random walks [15] . Both advantages simplify the complexity of the solution.

Now, our objective is to compute the green function $G_{d_{1\downarrow},d_{1\downarrow}^\dagger}(\omega)$. For this we take the graph $\mathscr{G}_{d_1d_2}$ associated to the matrix (4.13). See Figure 4.1.a). The vertexes of this graph are the operators in the first site of the of the green functions $(d_{1\downarrow},d_2,c_k.\ d_1^\dagger)$. $d_1^\dagger$ is not included since it only appears in the second sub-index of the green functions. The edges are given by the non-diagonal sites in the matrix. In addition, an energy parameter is assigned to each vertex, according to the corresponding term in the diagonal. These energies can also be thought as the magnitude of edges connecting each vertex with itself. The plot of the energy parameters in this algorithm is quite important, hence we prefer to keep this name to differentiate them from the other couplings.

The algorithm consists in the following. Each step of Gauss-Jordan elimination leads to a new graph with different energies and couplings. The elimination of a row and column is equivalent to pop the corresponding vertex in the graph. For instance, lets eliminate the first row and column of the matrix in (4.13). For it we just need to subtract the rank-1 matrix with the same first row and first column

$$\begin{bmatrix}\omega-\varepsilon_k & -V_2 & -V_1\\ -V_2^* & \omega-\varepsilon_2 & -t_{dots}\\ -V_1^* & -t_{dots}^* & \omega-\varepsilon_1\end{bmatrix}-\begin{bmatrix}\omega-\varepsilon_k & -V_2 & -V_1\\ -V_2^* & \frac{V_2^*V_2}{\omega-\varepsilon_k} & \frac{V_2^*V_1}{\omega-\varepsilon_k}\\ -V_1^* & \frac{V_2V_1^*}{\omega-\varepsilon_k} & \frac{V_1^*V_1}{\omega-\varepsilon_k}\end{bmatrix}=\begin{bmatrix}0 & 0 & 0\\ 0 & \omega-\varepsilon_2-\frac{V_2^*V_2}{\omega-\varepsilon_k} & -t_{dots}-\frac{V_2^*V_1}{\omega-\varepsilon_k}\\ 0 & -t_{dots}^*-\frac{V_2V_1^*}{\omega-\varepsilon_k} & \omega-\varepsilon_1-\frac{V_1^*V_1}{\omega-\varepsilon_k}\end{bmatrix} \tag{4.14}$$

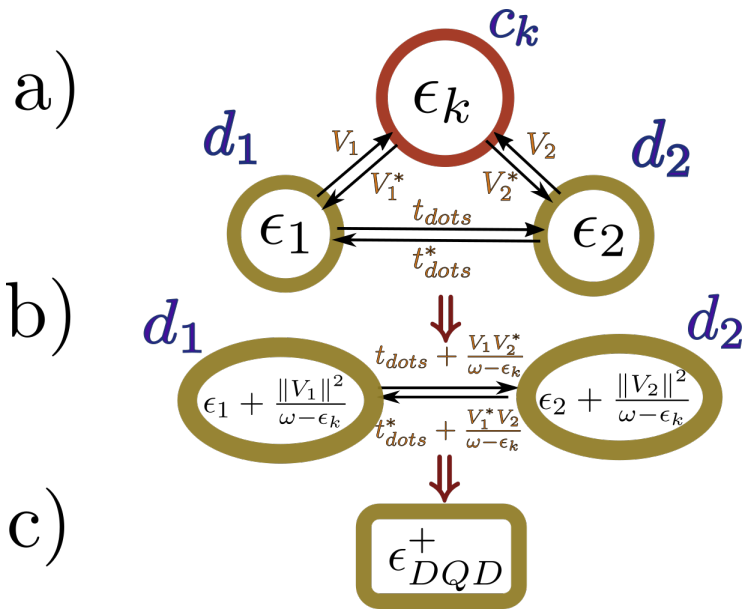

Figure 4.1: Graph representation of Gauss-Jordan elimination a) Graph $\mathscr{G}_{d_1 d_2}$ b) After the elimination of vertex c_k, the energies of dots d_1 and d_2, and the coupling parameter are changed. c) After Gaussian elimination of dot 2 the energy of the remaining dot $\varepsilon_D QD^+$ represents the transport information through d_1 of the entire DQD.

Source: *By the author.*

The graph associated to this matrix can be observed in Figure 4.1.b) where operator c_k has been popped out of the graph. It is possible to associate the correction to the the energies and couplings to the possible walks passing through the vertex c_k. For instance d_1's energy ε_1 receives an extra-term $\frac{V_1^* V_1}{\omega - \varepsilon_k}$ representing an additional walk from d_1 to d_1 passing through c_k. The same logic can be applied to the other terms coupling terms. The correction to t_dots is $\frac{V_1^* V_2}{\omega - \varepsilon_k}$ which corresponds to a path from d_1 to d_2 passing through the popped vertex c_k. Note that this term includes the multiplication both couplings with the vertex divided by the difference of ω with the energy of the vertex. This correspondence between the energy correction and eliminated paths through the graph makes the "popping" process an straightforward task.

We now proceed to pop vertex d_2 which leaves just a single vertex as shown in Figure 4.1.c). The energy of it can be readily computed with the previous path elimination idea which gives

$$\varepsilon^+_{DQD} = \varepsilon_1 + \sum_{\mathbf{k}} \frac{V_1 V_1^*}{\omega - \varepsilon_{\mathbf{k}}} + \frac{\left\| t_{dots} + \sum_{\mathbf{k}} \frac{V_1 V_2^*}{\omega - \varepsilon_{\mathbf{k}}} \right\|^2}{\omega - \varepsilon_2 - \sum_{\mathbf{k}} \frac{V_2 V_2^*}{\omega - \varepsilon_{\mathbf{k}}}}, \tag{4.15}$$

where we selectively included the $\sum_k$-terms in the places where k appeared.

As a result of Gauss-Jordan elimination the linear equation in 4.13 has evolved into the trivial form

$$\begin{bmatrix} 0 & 0 & 0 \\ 0 & 0 & 0 \\ 0 & 0 & \omega - \varepsilon^{+}_{DQD} \end{bmatrix} \begin{bmatrix} G_{c_{\mathbf{k}},d_1^\dagger}(\omega) \\ G_{d_2,d_1^\dagger}(\omega) \\ G_{d_1,d_1^\dagger}(\omega) \end{bmatrix} = \begin{bmatrix} 0 \\ 0 \\ 1 \end{bmatrix}. \tag{4.16}$$

The Green function is then

$$G_{d_1,d_1^\dagger}(\omega) = \frac{1}{\omega - \varepsilon^{+}_{DQD}} = \left[\left(\omega - \varepsilon_1 - \sum_{\mathbf{k}} \frac{V_1 V_1^*}{\omega - \varepsilon_{\mathbf{k}}} \right) - \frac{\left(t_{dots} + \sum_{\mathbf{k}} \frac{V_1 V_2^*}{\omega - \varepsilon_{\mathbf{k}}} \right) \left(t_{dots} + \sum_{\mathbf{k}} \frac{V_1 V_2^*}{\omega - \varepsilon_{\mathbf{k}}} \right)^*}{\omega - \varepsilon_2 - \sum_{\mathbf{k}} \frac{V_2 V_2^*}{\omega - \varepsilon_{\mathbf{k}}}} \right]^{-1}. \tag{4.17}$$

This Green function will be very important in the following chapters where we will compare its behavior with the green function of a Majorana mode.

4.1.2 Graph Algorithm

In this part we summarize the steps of the graph algorithm in order to apply them later to more complicated systems:

1. Computing the transport equations with the second term fixed in the creation operator of $d^\dagger$.
2. Writing the graph associated to the transport system. The vertexes are the operators in the first site of the of the green functions. Energies and couplings are associated to the vertex and edge numbers of the graphs respectively.
3. Popping the vertexes of the graph. Each vertex popping involves the following steps.
   (a) Computing the extra-terms in the energies and couplings based on the walks passing through the popped vertex.
   (b) Eliminating this vertex from the graph.
   (c) Iterating till there is only the vertex d.
4. The energy in the remaining vertex d is $\varepsilon_d = \frac{1}{\omega - G_{d,d^\dagger}(\omega)}$.

This algorithm will be our main method to find the green function and therefore the density of states of any interacting system.

4.1.3 Ballistic transport in a double quantum dot

In this subsection we describe the remaining steps to extract the density of states of the double quantum dot from the Green function 4.17. We will plot the results and observe the evolution of the DOS while tuning the parameters of the model.

First note that equation (4.17) depends on the term $\sum_k \frac{V_i^* V_j}{\omega - \varepsilon_k}$ which describes the broadening of the DOS when the QD enters in contact with the lead. This broadening is usually named $\Gamma_i = V_i^* V_i$ (Or Δ depending on the text book). In general V_i is a function of $\mathbf{k}$. However, in the limit of flat-band we can assume that V_i is constant. Therefore, it is enough to integrate

$$\sum_k \frac{1}{\omega - \varepsilon_k + is} = \int_{-D}^{D} \frac{d\varepsilon_k}{\omega - \varepsilon_k + is} = -\ln\left(\frac{D - \varepsilon_k + is}{-D - \varepsilon_k + is}\right) \xrightarrow[D\to\infty]{} -i, \tag{4.18}$$

where we assumed that there is a maximum energy cutoff D going to infinity in the wide-band limit. Hence

$$-i\Gamma_i = \sum_k \frac{V_i^* V_i}{\omega - \varepsilon_k}. \tag{4.19}$$

We can replace this in equation (4.17) to obtain the real expression for the green function $G_{d_1, d_1^\dagger}(\omega)$. The terms of the form $V_1 V_2^*$ can be replaced for $\sqrt{\Gamma_1 \Gamma_2}$, supposing there is no additional complex phase.

Now, remember from (4.8) that the DOS ρ depends on the imaginary factor of the Green Function $G_{d_1, d_1^\dagger}(\omega)$. This term depends in the broadening Γ. If $\Gamma = 0$ the density of states will be 0 as well. At any other case, one of the dots should be attached to the lead. Let Γ_1 be the broadening of this dot. We will take Γ_1 as our natural unit for the rest of this thesis. In Figure 4.2 we can observe the evolution of the Density of States under certain processes. Each plot includes an inset showing the model applied to the figure. The coupling in purple indicates the tuning variable. We set $e_1 = e_2 = 0$ so that both dots satisfy PHS. The primary results are the

1. **Coupling QD2. Figure 4.2(a)(b):** At $\Gamma_2 = 0$ the second dot is decoupled, hence the first dot's DOS is the same of a single dot case. The maximum height is achieved at $\rho\pi\Gamma_1 = 1$ and the width of this peak is about Γ_1, just as in Figure Figure 3.2. When the second dot is attached $\Gamma_2 > 0$ the density of states is divided between both dots. At $\Gamma_1 = \Gamma_2$ the DOS at the Fermi energy is equal to $\frac{1}{4\pi\Gamma}$ for both dots.

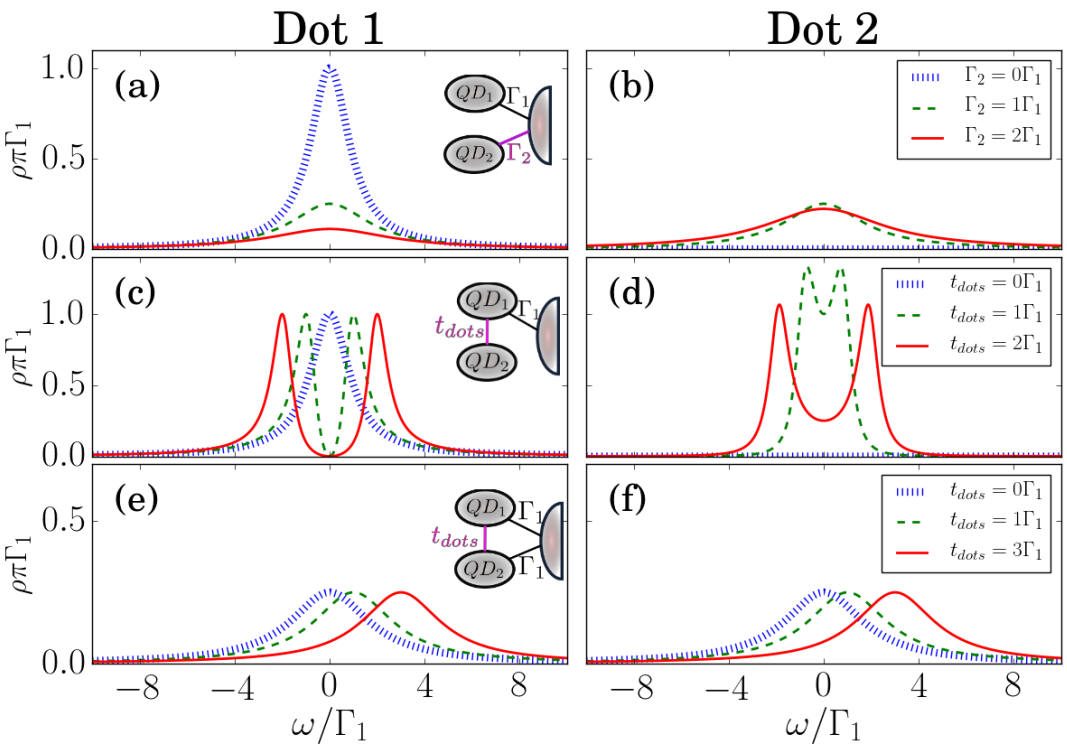

Figure 4.2: Evolution of the density of states at each QD (Left: dot 1, Right: dot 2) at three distinct arrangements of DQD-lead coupling. The inset at the first column depicts the type of coupling. The purple line represents the tuning variable. The energy unit is Γ_1. $e_1 = e_2 = 0$ in all arrangements. (a),(b) The lead is connected to both QDs. Tuning variable: Γ_2. (c)(d) Indirect coupling of the second dot through dot one. Tuning variable: $\_dots$. (e)(f) Triangular coupling. Tuning variable: t_{dots}.

Source: *By the Author*

2. **Indirect Coupling of QD2. Figure 4.2(c)(d):** This is case is interesting. When the second dot is connected indirectly through the first dot, quantum inference splits the central peak in two new states. We will observe later that in the interacting case this procedure can also destroy the Kondo signature.

3. **Breaking Particle Hole Symmetry. Figure 4.2(e)(f):** Suppose we have $\Gamma_2 = \Gamma_1$. The "triangular connections" break Particle Hole Symmetry. The central peak is displaced to the positive part of the spectrum. Contrary to the previous case, this situation will be avoided during this project. This is because this PHS-breaking will prevent the Majorana to tunnel inside the DQD.

4.2 The Numerical Renormalization Group (NRG)

At low energies a renormalization group approach is necessary to deal with the effects of high correlations. This implies that the divergent resistivity in Kondo model will be renormalized to a finite quantity.

In the 1970's G.Wilson created a numerical method to solve the Anderson model . This method receives the name of Numerical Renormalization Group (NRG) [16, 17, 18]. It consists of three basic steps :

1. To perform a numerical discretization of the energy spectrum in logarithmic intervals.
2. To map the discretized model onto a semi-infinity chain Hamiltonian.
3. To diagonalize iteratively the chain hamiltonian .

The final result will be the spectrum of the Hamiltonian. Other important properties of the material such as density of states, conductivity, specific heat, susceptibility can also be computed. On this project we are mainly interested in the Density of States (DOS). The method used to compute the DOS is the Density Matrix numerical renormalization Group (DM-NRG). A complete description of this algorithm will be given in the followin sections.

For now, we proceed to describe how the NRG is applied to solve the Anderson model in a QD:

Note *I still need to do a long revision to this section. Probably I will send most of the computations to the abstract and leave a summary of NRG and its advantages in the main text.*

Logarithmic Discretization:

We start with an Anderson model hamiltonian such as the one in (3.3) without magnetic field

$$H = \frac{U}{2} + \sum_{\sigma}\left[\left(\varepsilon_d + \frac{U}{2}\right) d_\sigma^\dagger d_\sigma + \frac{U}{2}(d_\sigma^\dagger d_\sigma - 1)^2 + \sum_{\mathbf{k}} \varepsilon_{\mathbf{k}} c_{\mathbf{k}\sigma}^\dagger c_{\mathbf{k}\sigma} + V_{\mathbf{k}} d_\sigma^\dagger c_{\mathbf{k}\sigma} + V_{\mathbf{k}}^* c_{\mathbf{k}\sigma}^\dagger d_\sigma\right]. \tag{4.20}$$

At low-energies we can assume that QD couples only to s-wave states in the leads[18]. This implies that that the Fermi surface is contained in a single, isotropic conduction band extending inside some fixed cutoffs $-D$ and D. Thus, $\varepsilon_{\mathbf{k}}$ only depends on $|\mathbf{k}|$. This makes possible to transform the sum over $\mathbf{k}$ in equation 4.20 into an integral over ε between the energy cutoffs

$$\begin{aligned} H \quad = \sum_\sigma \quad & \left[\left(\varepsilon_d + \frac{U}{2}\right) d_\sigma^\dagger d_\sigma + \frac{U}{2}(d_\sigma^\dagger d_\sigma - 1)^2 + \int_{-D}^{D} \mathrm{d}\varepsilon\ \varepsilon c_{\varepsilon\sigma}^\dagger c_{\varepsilon\sigma} \right. \\ & \left. + \int_{-D}^{D} \sqrt{\rho_\sigma(\varepsilon)}\mathrm{d}\varepsilon\ V_\varepsilon d_\sigma^\dagger c_{\mathbf{k}\sigma} + V_\varepsilon^* c_{\varepsilon\sigma}^\dagger d_\sigma\right]. \end{aligned} \tag{4.21}$$

Here $c^{\dagger}_{\varepsilon\sigma}$ creates an electron with energy ε and $\rho_\sigma(\varepsilon)$ is the density of states of the system per spin, which appears in the integral due to the change of variable from $\mathbf{k}$ to $\varepsilon \propto |\mathbf{k}|^2$. Finally, we ignore the energy dependence of ρ and V_d and we replace them by their values in the Fermi energy (This approximation has no great relevance which is justified in [18]) and we renormalize the energy band doing the replacements $k = \frac{\varepsilon}{D}$ and $c_{k\sigma} := \sqrt{D} c_{\varepsilon\sigma}$ so that (4.21) becomes

$$H = D\sum_\sigma \left[\frac{1}{D}\left(\varepsilon_d + \frac{U}{2}\right) d^{\dagger}_\sigma d_\sigma + \frac{U}{2D}(d^{\dagger}_\sigma d_\sigma - 1)^2 + \int_{-1}^{1} \mathrm{d}k\, k c^{\dagger}_{k\sigma} c_{k\sigma} \right. \\ \left. + \sqrt{\frac{\Gamma}{\pi D}} \int_{-1}^{1} \mathrm{d}k\, d^{\dagger}_\sigma c_{k\sigma} + c^{\dagger}_{k\sigma} d_\sigma \right] \tag{4.22}$$

$$= H_d + D\sum_\sigma \left[\int_{-1}^{1} \mathrm{d}k\, k c^{\dagger}_{k\sigma} c_{k\sigma} + \sqrt{\frac{\Gamma}{\pi D}} \int_{-1}^{1} \mathrm{d}k\, d^{\dagger}_\sigma c_{k\sigma} + c^{\dagger}_{k\sigma} d_\sigma \right], \tag{4.23}$$

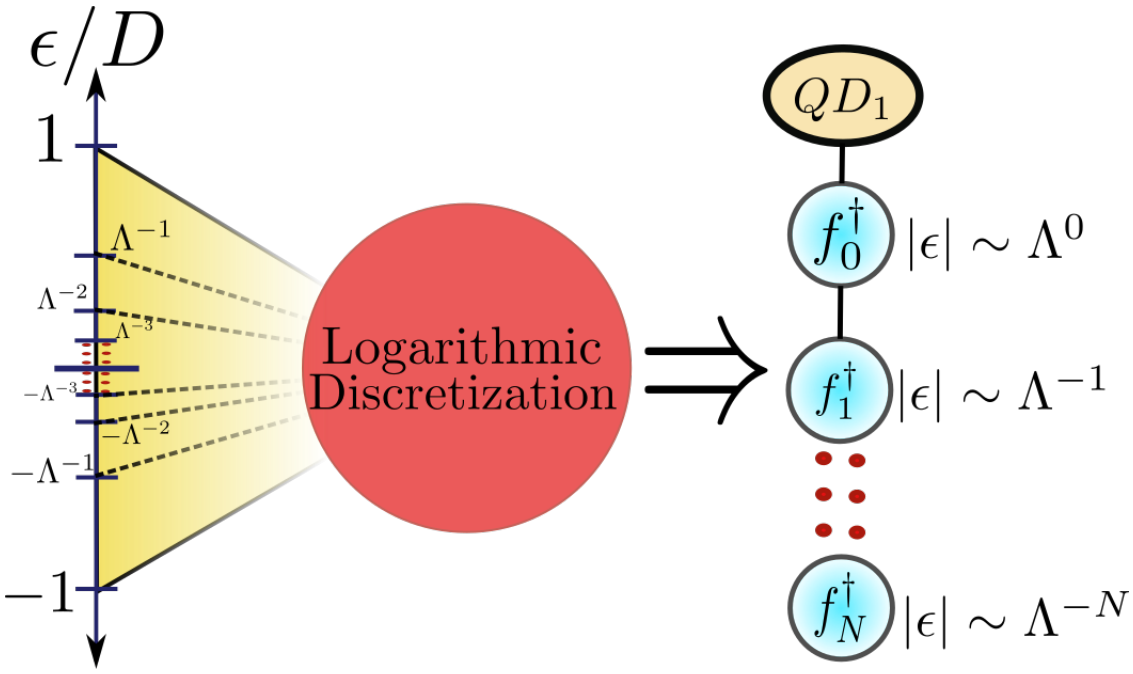

Figure 4.3: . Energy interval discretization. Source: *By the Author*

where $\Gamma = \pi\rho V^2$ is associated to the lever-width [11, (3.5)]. At this point we have our model dependent of three unit-less constants $\frac{\varepsilon_d}{D}$, $\frac{U}{2D}$ and $\frac{\Gamma}{\pi D}$. The logarithmic discretization starts by defining an scaling parameter $\Lambda \geq 1$ in diving the energy domain $[-1, 1]$ into an array

of intervals of the form $\{[\pm\Lambda^{-(n+1)}, \pm\Lambda^n]\}_{n\in\mathbb{N}}$, as we can observe in Figure 4.3. Note that the width of these intervals is decreasing exponentially by

$$d_n = \Lambda^{-n}\left(1-\Lambda^{-1}\right).$$

Then inside of these energy intervals we can define a set of orthonormal Fourier series of the form

$$\phi_{np}^{\pm}(\varepsilon) = \begin{cases} \frac{1}{\sqrt{d_n}} e^{\pm i\omega_n p\varepsilon} & \varepsilon \in [\pm\Lambda^{-(n+1)}, \pm\Lambda^n] \\ 0 & \text{a.o.c}\ , \end{cases} \tag{4.24}$$

with $\omega_n := \frac{2\pi}{d_n}$ so that $\phi_{np}^{\pm}\left(\pm\Lambda^{-(n+1)}\right) = \phi_{np}^{\pm}\left(\pm\Lambda^{-n)}\right)$. Then we can decompose the creation operators $c_k^\dagger$ into their interval-Fourier contributions as

$$c_{k\sigma}^\dagger = \sum_{np} \phi_{np}^{+}(k) c_{np\sigma}^{+\dagger} + \phi_{np}^{-}(k) c_{np\sigma}^{-\dagger} \tag{4.25}$$

with the new creation operators defined as

$$c_{np\sigma}^{\pm\dagger} := \left(c_{np\sigma}^{\pm}\right)^\dagger = \int_{-1}^{1} \mathrm{d}\varepsilon\ \left[\phi_{np}^{+}(\varepsilon)\right]^* c_{\varepsilon\sigma}^\dagger.$$

This decomposition (4.25) is a simple consequence of the orthonormality of the functions defined in (4.24). In addition we can readily proof that $c_{np\sigma}^{\pm\dagger}$-operators satisfy the anti-commutation relations, so that they are rightful fermionic creation operators.

We can now use (4.25) to replace the k-dependent terms in hamiltonian (4.22). Then we obtain

$$\begin{aligned}
\int_{-1}^{1} \mathrm{d}k\ c_{k\sigma}^\dagger d_\sigma &= \int_{-1}^{1} \mathrm{d}k\ \left(\sum_{np} \phi_{np}^{+}(k) c_{np\sigma}^{+\dagger} + \phi_{np}^{-}(k) c_{np\sigma}^{-\dagger}\right) d_\sigma \\
&= \left(\sum_{np} \left(\int_{-1}^{1} \mathrm{d}k\ \phi_{np}^{+}(k)\right) c_{np\sigma}^{+\dagger} + \left(\int_{-1}^{1} \mathrm{d}k\ \phi_{np}^{-}(k)\right) c_{np\sigma}^{-\dagger}\right) d_\sigma \\
&= \left(\sum_{np} \left(\int_{\Lambda^{-(n+1)}}^{\Lambda^{-n}} \mathrm{d}k\ \frac{e^{i\omega_n pk}}{\sqrt{d_n}}\right) c_{np\sigma}^{+\dagger} + \left(\int_{-\Lambda^{-n}}^{-\Lambda^{-(n+1)}} \mathrm{d}k\ \frac{e^{-i\omega_n pk}}{\sqrt{d_n}}\right) c_{np\sigma}^{-\dagger}\right) d_\sigma \\
&= \left(\sum_{np} \sqrt{d_n}\delta_p c_{np\sigma}^{+\dagger} + \sqrt{d_n}\delta_p c_{np\sigma}^{-\dagger}\right) d_\sigma \\
&= \sqrt{1-\Lambda^{-1}} \sum_{n} \Lambda^{-\frac{n}{2}} \left(c_{np\sigma}^{+\dagger} + c_{np\sigma}^{-\dagger}\right) d_\sigma.
\end{aligned} \tag{4.26}$$

And

$$
\begin{aligned}
\int_{-1}^{1} \mathrm{d}k\, k c_{k\sigma}^{\dagger} c_{k\sigma} &= \sum_{n,n',p,p'} \sum_{s,s'=\pm} \left(\int_{-1}^{1} k\mathrm{d}k\, \phi_{np}^{s}(k) \left(\phi_{np}^{s'}(k) \right)^{*} \right) c_{np\sigma}^{s\dagger} c_{n'p'\sigma}^{s'} \\
&= \sum_{n,n',p,p'} \sum_{s,s'=\pm} \left(\frac{\delta_{nn'}\delta_{ss'}}{d_n} \int_{\Lambda^{-(n+1)}}^{\Lambda^{-n}} k\mathrm{d}k\, e^{is\omega_n k(p-p')} \right) c_{np\sigma}^{s\dagger} c_{np'\sigma}^{s} \\
&= \sum_{npp'} \sum_{s=\pm} \left(\frac{s}{2}\Lambda^{-2n}\left(1-\Lambda^{-2}\right)\delta_{pp'} + \frac{1-\delta_{pp'}}{is\omega_n (p-p')} \left[k e^{is\omega_n k(p-p')} \right]_{\Lambda^{-(n+1)}}^{\Lambda^{-n}} \right) \frac{c_{np\sigma}^{s\dagger} c_{np'\sigma}^{s'}}{d_n} \\
&= \frac{1}{2}\left(1+\Lambda^{-1}\right) \sum_{np} \Lambda^{-n} \left(c_{np\sigma}^{+\dagger} c_{np\sigma}^{+} - c_{np\sigma}^{-\dagger} c_{np\sigma}^{-} \right) \\
&\quad + \sum_{n} \sum_{p\neq p'} \frac{1-\Lambda^{-1}}{2i\pi (p'-p)} \left(c_{np\sigma}^{+\dagger} c_{np'\sigma}^{+} - c_{np'\sigma}^{-\dagger} c_{np\sigma}^{-} \right) e^{\frac{2i\pi(p-p')}{1-\Lambda^{-1}}}.
\end{aligned} \tag{4.27}
$$

Thus, if we replace (4.26) and (4.27) into (4.22) we will obtain a logarithmic discretization of the hamiltonian. The next part will we to map this discretization to an iterative process that is worth for a numerical computations.

Mapping the Anderson model to a Chain-Hamiltonian

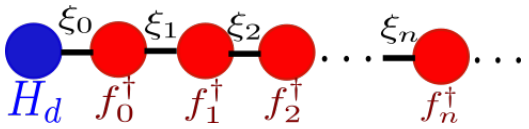

Figure 4.4: Chain-Hamiltonian describing the Anderson model. The chain starts at the initial dot hamiltonian H_d. The $f_m^\dagger$'s are the creation operators at the n^{th}-site of the chain. The ξ_n's describe the magnitude of the interaction between consecutive sites.

We are looking for a model just like the one we have in Figure 4.4. This is because a Chain-Hamiltonian will give an iterative approximation of the Anderson model with an increasing (but still controllable) number of degrees of freedom. This will provide the rightful structure for a numerical diagonalization of the hamiltonian.

To do this, observe from equations (4.26),(4.27) that the QD (d_σ) couples directly only to the operators with $p = 0\left(c_{n0\sigma}^{\pm\dagger}\right)$. The $p \neq 0$ terms will appear in the hamiltonian only because they are coupled to $c_{np\sigma}^{+\dagger}$ in Equation (4.27). Thus, as a first approximation we can neglect all terms in (4.27) with $p \neq 0$. This leaves only the first part of (4.27), so that we can define

$c^{\pm\dagger}_{n\sigma} := c^{\pm\dagger}_{np\sigma}$. Let

$$f^{\dagger}_{0\sigma} = \sqrt{\frac{1-\Lambda^{-1}}{2}} \sum_n \Lambda^{-\frac{n}{2}} \left(c^{+\dagger}_{n\sigma} + c^{-\dagger}_{n\sigma}\right), \text{ so that } \sqrt{2} f^{\dagger}_{0\sigma} d_\sigma = \int_{-1}^{1} \mathrm{d}k \; c^{\dagger}_{k\sigma} d_\sigma. \tag{4.28}$$

Note $\left\{f^{\dagger}_{0\sigma}, f_{0\sigma}\right\} = \frac{1-\Lambda^{-1}}{2} \sum_n 2\Lambda^{-n} = 1$. Replacing this in (4.22)we get

$$H = H_d + D \sum_\sigma \left[\sqrt{\frac{2\Gamma}{\pi D}} \left(d^{\dagger}_\sigma f_{0\sigma} + f^{\dagger}_{0\sigma} d_\sigma\right) + \frac{1}{2}\left(1+\Lambda^{-1}\right) \sum_n \Lambda^{-n} \left(c^{+\dagger}_{n\sigma} c^{+}_{n\sigma} - c^{-\dagger}_{n\sigma} c^{-}_{n\sigma}\right) \right].$$

$f^{\dagger}_0$will represent the first site of the chain-hamiltonian in Figure 4.4 since no other term is coupled to the dot hamiltonian. We also have the coupling term $\xi_0 = \sqrt{\frac{2\Gamma}{\pi D}}$. It is possible to obtain the following $f^{\dagger}_m$-operators by supposing a solution of the form

$$f^{\dagger}_{m\sigma} = \sum_n a^{+}_{mn} c^{+\dagger}_{n\sigma} + a^{-}_{mn} c^{-\dagger}_{n\sigma} = \sum_n \sum_{s=\pm} a^{s}_{mn} c^{s\dagger}_{n\sigma}, \tag{4.29}$$

such that they satisfy the anti-commutation relations

$$\left\{f^{\dagger}_{m\sigma}, f_{m\sigma}\right\} = \delta_{mm'}\delta_{\sigma\sigma'} \; , \; \left\{f^{\dagger}_{m\sigma}, f^{\dagger}_{m\sigma}\right\} = \left\{f^{\dagger}_{m\sigma}, f^{\dagger}_{m\sigma}\right\} = 0$$

and

$$\frac{1}{2}\left(1+\Lambda^{-1}\right) \sum_n \Lambda^{-n} \left(c^{+\dagger}_{n\sigma} c^{+}_{n\sigma} - c^{-\dagger}_{n\sigma} c^{-}_{n\sigma}\right) = \sum_{m=0}^{\infty} \Lambda^{\frac{-m}{2}} \xi_m \left(f^{\dagger}_{m\sigma} f_{m+1,\sigma} + f^{\dagger}_{m+1\sigma} f_{m\sigma}\right). \tag{4.30}$$

It is possible to find a solution for this system using the formula of the right part of equation 4.30. Since the relation is only given between consecutive terms $m, m+1$ and we already have the coefficients for $m=0$ $\left(a^{s}_{0n} = \sqrt{\frac{1-\Lambda^{-1}}{2}}\Lambda^{-\frac{n}{2}}\right)$. Then it is possible to determine the upper coefficients in a recursive way starting from $m=0$. Supposing we can obtain the m^{th}-coefficients (a^{s}_{mn}) and then finding iteratively the coefficients of $m+1$ (a^{s}_{mn}) using the relation given by equation (4.30). This provides a numerical way for obtaining the $f^{\dagger}_{m\sigma}$ operators. In fact in our case, where we actually did important assumptions, the problem can be solved analytically obtaining that the final hamiltonian is given by

$$H = H_d + D \sum_\sigma \left[\sqrt{\frac{2\Gamma}{\pi D}} \left(d^{\dagger}_\sigma f_{0\sigma} + f^{\dagger}_{0\sigma} d_\sigma\right) + \frac{1}{2}\left(1+\Lambda^{-1}\right) \sum_{n=0}^{\infty} \Lambda^{\frac{-n}{2}} \xi_n \left(f^{\dagger}_{n\sigma} f_{n+1,\sigma} + f^{\dagger}_{n+1\sigma} f_{n\sigma}\right) \right]. \tag{4.31}$$

with

$$\xi_n = \frac{1-\Lambda^{-n-1}}{\left(1-\Lambda^{-2n-1}\right)^{\frac{1}{2}} \left(1-\Lambda^{-2n-3}\right)^{\frac{1}{2}}}.$$

The formal recursive-solution of this problem can be found in [16] . Note that equation (4.31) describes the chain hamiltonian model that we where looking for in Figure 4.4. Note that in the limit when $n \longrightarrow \infty$

$$\Lambda^{\frac{-n}{2}}\xi_n \longrightarrow \frac{\Lambda^{\frac{-n}{2}}(1-\Lambda^{-n})}{1-\Lambda^{-2n}} \sim \frac{\Lambda^{\frac{-n}{2}}}{1+\Lambda^{-n}},$$

which implies an exponential decaying of the hopping term in the chain.

Iterative Diagonalization in a Single QD process

Now that we have an iterative representation of the Anderson Model Hamiltonian (4.31), lets take a look to how the NRG code would work for a QD. We start with the dot hamiltonian. (Since the D term is always present as a normalizing factor, we are going to avoid this term in future computations and suppose that we are working with unit-less variables ε_d, U and $\Gamma' := \sqrt{\frac{2\Gamma}{\pi D}}$).

$$H_d = \frac{1}{D}\left(\varepsilon_d + \frac{U}{2}\right) d^\dagger_\sigma d_\sigma + \frac{U}{2D}(d^\dagger_\sigma d_\sigma - 1)^2. \tag{4.32}$$

Now observe that hamiltonian 4.32 already has a diagonal form in the base $\{|\uparrow\downarrow\rangle, |\uparrow\rangle, |\downarrow\rangle, |0\rangle\}$

$$H_d = \frac{1}{D}\begin{bmatrix} 2\varepsilon_d + \frac{3U}{2} & 0 & 0 & 0 \\ 0 & \varepsilon_d + \frac{U}{2} & 0 & 0 \\ 0 & 0 & \varepsilon_d + \frac{U}{2} & 0 \\ 0 & 0 & 0 & \frac{U}{2} \end{bmatrix}.$$

Lets define $H_{-1} = \Lambda^{\frac{-1}{2}} H_d$. Adding the first chain interaction to H_d we obtain a new hamiltonian of the form

$$H_0 = \Lambda^{\frac{1}{2}} H_{-1} + \Gamma'\left(d^\dagger_\sigma f_{0\sigma} + f^\dagger_{0\sigma} d_\sigma\right). \tag{4.33}$$

The Hilbert space for this hamiltonian has to be extended to include the 4 degrees of freedom of the $f^\dagger_{0\sigma}$ particles which are also given by $\{|\uparrow\downarrow\rangle, |\uparrow\rangle, |\downarrow\rangle, |0\rangle\}$. Therefore the total Hilbert space for H_0 is given by a base of the form

$$|s_1\rangle|s_2\rangle := |s_1\rangle \otimes |s_2\rangle \text{ with } |s_{1,2}\rangle \in \{|\uparrow\downarrow\rangle, |\uparrow\rangle, |\downarrow\rangle, |0\rangle\}.$$

This gives an space of dimension $4 \times 4 = 16$. Now before adventuring to write the hamiltonian for H_0 as a 16×16-matrix note that H_0 preserves particle number N and the total spin S. Therefore we can use N and S as quantum numbers and generate the Hamiltonian H_0 in blocks. We will observe that the terms in the diagonal will correspond to the eigenvalues of H_{-1} for the first space. The non-diagonal terms are the result of the hopping interactions with the first site.

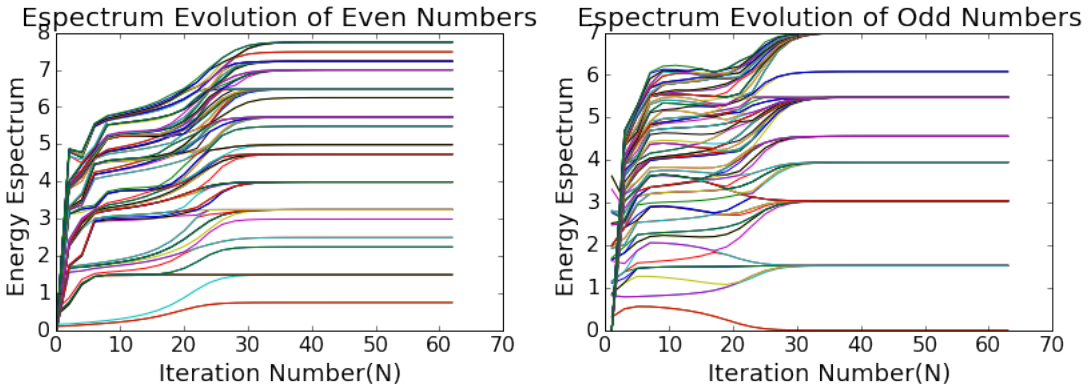

(a) N takes only even values

(b) N run only through odd values

Figure 4.5: Evolution of the QD-spectrum vs number of iterations of the code for $U = 0.5$, $e_d = -0.25$, $\Gamma = 2.82 \times 10^{-2}$.

$H_{N=0,S=0}$:

$$|0\rangle|0\rangle \rightarrow \quad \left[\tfrac{U}{2}\right]$$

$H_{N=4,S=0}$:

$$|\uparrow\downarrow\rangle|\uparrow\downarrow\rangle \rightarrow \quad \left[2\varepsilon_d + \tfrac{3U}{2}\right]$$

$H_{N=1,S=\frac{1}{2}}$:

$$\begin{matrix} |\uparrow\rangle|0\rangle \rightarrow \\ |0\rangle|\uparrow\rangle \rightarrow \end{matrix} \begin{bmatrix} \varepsilon_d + \frac{U}{2} & \Gamma' \\ \Gamma' & \frac{U}{2} \end{bmatrix}$$

$H_{N=1,S=\frac{-1}{2}}$:

$$\begin{matrix} |\uparrow\rangle|0\rangle \rightarrow \\ |0\rangle|\uparrow\rangle \rightarrow \end{matrix} \begin{bmatrix} \varepsilon_d + \frac{U}{2} & \Gamma' \\ \Gamma' & \frac{U}{2} \end{bmatrix}$$

$H_{N=2,S=-1}$:

$$|\downarrow\rangle|\downarrow\rangle \rightarrow \quad \left[\varepsilon_d + \tfrac{U}{2}\right]$$

$H_{N=2,S=1}$:

$$|\uparrow\rangle|\uparrow\rangle \rightarrow \quad \left[\varepsilon_d + \tfrac{U}{2}\right]$$

$H_{N=2,S=0}$:

$$\begin{matrix} |\uparrow\downarrow\rangle|0\rangle \rightarrow \\ |\uparrow\rangle|\downarrow\rangle \rightarrow \\ |\downarrow\rangle|\uparrow\rangle \rightarrow \\ |0\rangle|\uparrow\downarrow\rangle \rightarrow \end{matrix} \begin{bmatrix} 2\varepsilon_d + \frac{3U}{2} & \Gamma & -\Gamma & 0 \\ \Gamma & \varepsilon_d + \frac{U}{2} & 0 & \Gamma \\ -\Gamma & 0 & \varepsilon_d + \frac{U}{2} & -\Gamma \\ 0 & \Gamma & -\Gamma & \frac{U}{2} \end{bmatrix}$$

$H_{N=3,S=\frac{1}{2}}$:

$$\begin{matrix} |\uparrow\downarrow\rangle|\uparrow\rangle \rightarrow \\ |\uparrow\rangle|\uparrow\downarrow\rangle \rightarrow \end{matrix} \begin{bmatrix} \varepsilon_d + \frac{U}{2} & -\Gamma' \\ -\Gamma' & \frac{U}{2} \end{bmatrix}$$

$H_{N=3,S=\frac{-1}{2}}$:

$$\begin{matrix} |\uparrow\downarrow\rangle|\downarrow\rangle \rightarrow \\ |\downarrow\rangle|\uparrow\downarrow\rangle \rightarrow \end{matrix} \begin{bmatrix} \varepsilon_d + \frac{U}{2} & -\Gamma' \\ -\Gamma' & \frac{U}{2} \end{bmatrix}$$

Finally, we proceed to diagonalize H_0 by blocks $H_{N,S}$. The resulting eigenvectors will be characterized by both quantum numbers so that we can write them in the form $|N,S,i\rangle$ with i

takes as many values as the degeneracy of its block. For higher values of N, the general formula for equation (4.33) looks as

$$H_{N+1} = \Lambda^{\frac{1}{2}} \left[H_N + \frac{1}{2} \left(1 + \Lambda^{-1}\right) \xi_N \left(f^{\dagger}_{N\sigma} f_{N+1,\sigma} + f^{\dagger}_{N+1\sigma} f_{N\sigma} \right) \right]. \tag{4.34}$$

We now proceed by induction supossing that for each N the Hamiltonian H_N is already diagonalized and the eigenvectors are organized in states with labels $|N,S,i\rangle$. The next step will be to add the 4-Hilbert space corresponding to $f_{N+1,\sigma}$ organized the eigenvectors according to the quantum numbers $|N',S',i\rangle$ and proceed to diagonalize by blocks the new Hamiltonian. Apart of it, the code must have a cutoff to the number of states.

This NRG code was previously implemented in C++ language by the advisor of this thesis. In Figure 4.5 we observe the evolution of the spectrum of the Hamiltonian according to the number of iterations of the code. As we can appreciate, this evolution converges for even and odd number around $N = 30$.

4.2.1 Density Matrix Renormalization Group (DM-NRG)

To compute dynamical quantities [19] like the density of states is the DMNRG [20]. Note *Sill planning this section*

4.2.2 NRG results in a Double Quantum Dot

We ran the NRG code for the DQD with the following set of parameters:

$$U_{1,2} = -2\varepsilon_{1,2} = 8.62\Gamma_1$$

Figure 4.6 shows the NRG results for the density of states of QD1 in different states. The three plots show the external Coulomb peaks at $e_1 = \frac{U}{2} \sim 8.62\Gamma_1$, which represent the DOS of the energy levels. In addition Figure 4.6a shows a central peak at the fermi energy. **This is the Kondo Peak**.

Figure 4.6b shows the DOS in the case where the two QDs are symmetrically attached. At low energies, the inset shows the appearance of two satellite peaks representing the Ruderman-Kittel-Kasuya-Yosida (RKKY) interaction. This interaction is explained for this particular case in section Appendix B.

Again, the most interesting case is in Figure 4.6c. The additional interference with the second dot completely destroys the Knondo effect. This effect is observed at energies closed to $t_{dots} = 0.689\Gamma$ and will take its relevance in the last chapter.

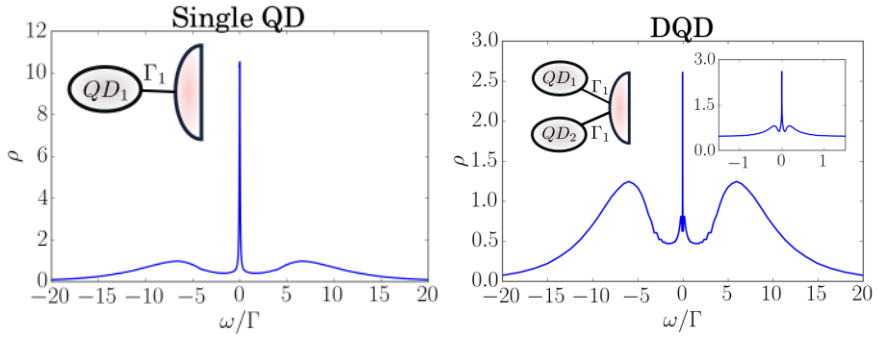

(a) (b) $\Gamma_2 = \Gamma_1$. Inset: Low energy DOS.

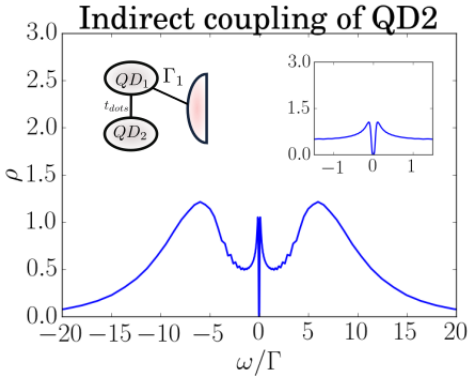

(c) $t_{dots} = 0.689\Gamma$. Low energy DOS.

Figure 4.6: Density of states in QD1 predicted by NRG at each case. The insets show the. Note that figure a) is in a different scale due to a major central peak ..

Source: *By the Author*

Bibliography

[1] A. Yu Kitaev. Unpaired Majorana fermions in quantum wires. *Phys.-Usp.*, 44(10S):131, 2001. ISSN 1063-7869. doi: 10.1070/1063-7869/44/10S/S29. URL http://stacks.iop.org/1063-7869/44/i=10S/a=S29. 1

[2] Jason Alicea. Majorana fermions in a tunable semiconductor device. *Phys. Rev. B*, 81 (12):125318, March 2010. doi: 10.1103/PhysRevB.81.125318. URL https://link.aps.org/doi/10.1103/PhysRevB.81.125318. 1

[3] Jason Alicea. New directions in the pursuit of Majorana fermions in solid state systems. *Rep. Prog. Phys.*, 75(7):076501, 2012. ISSN 0034-4885. doi: 10.1088/0034-4885/75/7/076501. URL http://stacks.iop.org/0034-4885/75/i=7/a=076501. 1

[4] Dong E. Liu and Harold U. Baranger. Detecting a majorana-fermion zero mode using a quantum dot. 84(20). ISSN 1098-0121, 1550-235X. doi: 10.1103/PhysRevB.84.201308. URL http://arxiv.org/abs/1107.4338. 1

[5] Minchul Lee, Jong Soo Lim, and Rosa Lopez. Kondo effect in a quantum dot side-coupled to a topological superconductor. 87(24):241402. doi: 10.1103/PhysRevB.87.241402. URL https://link.aps.org/doi/10.1103/PhysRevB.87.241402. 1

[6] E. Vernek, P. H. Penteado, A. C. Seridonio, and J. C. Egues. Subtle leakage of a majorana mode into a quantum dot. 89(16):165314. doi: 10.1103/PhysRevB.89.165314. URL https://link.aps.org/doi/10.1103/PhysRevB.89.165314. 1

[7] M. T. Deng, S. Vaitiekenas, E. B. Hansen, J. Danon, M. Leijnse, K. Flensberg, J. Nygard, P. Krogstrup, and C. M. Marcus. Majorana bound state in a coupled quantum-dot hybrid-nanowire system. 354(6319):1557–1562. ISSN 0036-8075, 1095-9203. doi: 10.1126/science.aaf3961. URL http://science.sciencemag.org/content/354/6319/1557. 1

[8] David A. Ruiz-Tijerina, E. Vernek, Luis G. G. V. Dias da Silva, and J. C. Egues. Interaction effects on a majorana zero mode leaking into a quantum dot. 91(11):115435. doi: 10.1103/PhysRevB.91.115435. URL https://link.aps.org/doi/10.1103/PhysRevB.91.115435. 1

[9] Alexander W. Holleitner, Robert H. Blick, Andreas K. HÃŒttel, Karl Eberl, and JÃ¶rg P. Kotthaus. Probing and Controlling the Bonds of an Artificial Molecule. *Science*, 297 (5578):70–72, July 2002. ISSN 0036-8075, 1095-9203. doi: 10.1126/science.1071215. URL http://science.sciencemag.org/content/297/5578/70. 3.1

[10] Dieter Bimberg, Marius Grundmann, and Nikolai N. Ledentsov. *Quantum Dot Heterostructures*. Wiley, Chichester, Eng.; New York, 1 edition, March 1999. ISBN 978-0-471-97388-1. 3.1, 3.1

[11] Michael Sindel. *Numerical Renormalization Group studies of Quantum Impurity Models in the Strong Coupling Limit*. Text.PhDThesis, Ludwig-Maximilians-UniversitÃt MÃŒnchen, January 2005. URL https://edoc.ub.uni-muenchen.de/3115/. 3.1, 3.3, 3.2, 3.4, 3.3, 4.2

[12] P. W. Anderson. Localized Magnetic States in Metals. *Physical Review*, 124(1):41–53, October 1961. doi: 10.1103/PhysRev.124.41. URL https://link.aps.org/doi/10.1103/PhysRev.124.41. 3.2

[13] W.J. de Haas, J. de Boer, and G.J. van dÃ«n Berg. The electrical resistance of gold, copper and lead at low temperatures. *Physica*, 1(7):1115 – 1124, 1934. ISSN 0031-8914. doi: https://doi.org/10.1016/S0031-8914(34)80310-2. URL http://www.sciencedirect.com/science/article/pii/S0031891434803102. 3.4

[14] Alexander Cyril Hewson. *The Kondo Problem to Heavy Fermions*. Cambridge University Press, April 1997. ISBN 978-0-521-59947-4. Google-Books-ID: fPzgHneNFDAC. 3.3, 3.3

[15] Daniel A Spielman. Algorithms, graph theory, and linear equations in laplacian matrices. In *Proceedings of the International Congress of Mathematicians*, volume 4, pages 2698–2722, 2010. URL http://www.mathunion.org/ICM/ICM2010.4/Main/icm2010.4.2698.2722.pdf. 4.1.1, 4.1.1

[16] Ralf Bulla, Theo A. Costi, and Thomas Pruschke. Numerical renormalization group method for quantum impurity systems. *Reviews of Modern Physics*, 80(2):395–450, April 2008. doi: 10.1103/RevModPhys.80.395. URL https://link.aps.org/doi/10.1103/RevModPhys.80.395. 4.2, 4.2

[17] Kenneth G. Wilson. The renormalization group: Critical phenomena and the Kondo problem. *Reviews of Modern Physics*, 47(4):773–840, October 1975. doi: 10.1103/RevModPhys.47.773. URL https://link.aps.org/doi/10.1103/RevModPhys.47.773. 4.2

[18] H. R. Krishna-murthy, J. W. Wilkins, and K. G. Wilson. Renormalization-group approach to the Anderson model of dilute magnetic alloys. 1. Static properties for the symmetric case. *Phys.Rev.*, B21:1003–1043, 1980. doi: 10.1103/PhysRevB.21.1003. 4.2, 4.2, 4.2

[19] T. A. Costi, A. C. Hewson, and V. Zlatic. Transport coefficients of the Anderson model via the numerical renormalization group. *Journal of Physics: Condensed Matter*, 6(13):2519, 1994. ISSN 0953-8984. doi: 10.1088/0953-8984/6/13/013. URL http://stacks.iop.org/0953-8984/6/i=13/a=013. 4.2.1

[20] Walter Hofstetter. Generalized Numerical Renormalization Group for Dynamical Quantities. *Physical Review Letters*, 85(7):1508–1511, August 2000. doi: 10.1103/PhysRevLett.85.1508. URL https://link.aps.org/doi/10.1103/PhysRevLett.85.1508. 4.2.1

[21] M. A. Ruderman and C. Kittel. Indirect Exchange Coupling of Nuclear Magnetic Moments by Conduction Electrons. *Physical Review*, 96(1):99–102, October 1954. doi: 10.1103/PhysRev.96.99. URL https://link.aps.org/doi/10.1103/PhysRev.96.99. B

[22] Kei Yosida. Magnetic Properties of Cu-Mn Alloys. *Physical Review*, 106(5):893–898, June 1957. doi: 10.1103/PhysRev.106.893. URL https://link.aps.org/doi/10.1103/PhysRev.106.893. B

Appendix A

Appendix

A.1 Proof of the Graph Method for Transport Equations.

Appendix B

Three peak appearance in the Double Quantum Dot model.

The DQD model is characterized by the formation of a new state that entangles the two Quantum dots through the leads. This produces an anti-ferromagnetic interaction between the QDs, commonly known as Ruderman-Kittel-Kasuya-Yosida (RKKY) interaction [21, 22]. As consequense, two satelite peaks will emerge in the Density of States.

To explain this phenomenon we will take a symmetric version of Hamiltonian (**??**) with $2e_i = U_i = U$, $t_i = t$ and $t_{dots} = 0$ for $i \in \{1,2\}$.

$$H = \sum_{i,k,\sigma} \frac{U_i}{2}(d^\dagger_{i\sigma}d_{i\sigma} - 1)^2 + t(d_{+,\downarrow} + d^\dagger_{+,\downarrow})\gamma_1 + \Gamma_i(d^\dagger_{i\sigma}c_{k\sigma} + c^\dagger_{k\sigma}d_{i\sigma}). \tag{B.1}$$

The symmetry of the previous Hamiltonian is suitable to apply a base change of the form

$$d_{+,\sigma} = \frac{1}{\sqrt{2}}(d_{1\sigma} + d_{2\sigma}) \ , \ d_{-,\sigma} = \frac{1}{\sqrt{2}}(d_{1\sigma} - d_{2\sigma}).$$

These new operators satisfy the fermionic anti-commutation relations

$$\{d_{\pm,\sigma}, d^\dagger_{\pm,\sigma}\} = 1, \{d_{\pm,\sigma}, d^\dagger_{\mp,\sigma}\} = 0,$$

so that the may be considered as fermion operators. All lineal terms in (B.1) are trivially adapted to the new base. The repulsion potential

$$\sum_i (\sum_\sigma d^\dagger_{i\sigma}d_{i\sigma} - 1)^2 = (\sum_\sigma d^\dagger_{1\sigma}d_{1\sigma} - 1)^2 + (\sum_\sigma d^\dagger_{2\sigma}d_{2\sigma} - 1)^2.$$

gives rise to a non-trivial interaction between the new states. To find this interaction we define the particle number operator

$$\hat{n}_{i,\sigma} := d^\dagger_{i,\sigma}d_{i,\sigma}.$$

So that

$$\hat{n}_{1,\sigma} = \frac{1}{2}\left(\hat{n}_{+,\sigma} + \hat{n}_{-,\sigma} + d^\dagger_{+,\sigma}d_{-,\sigma} + d^\dagger_{-,\sigma}d_{+,\sigma}\right) = \frac{1}{2}\left(\hat{N}_\sigma + \hat{E}_\sigma\right),$$

with $\hat{N} = \hat{n}_{+,\sigma} + \hat{n}_{-,\sigma}$ and $\hat{E}_\sigma = d^\dagger_{+,\sigma}d_{-,\sigma} + d^\dagger_{-,\sigma}d_{+,\sigma}$. Similarly

$$\hat{n}_{2,\sigma} = \frac{1}{2}\left(\hat{N}_\sigma - \hat{E}_\sigma\right).$$

Hence

$$\sum_i (\sum_\sigma d^\dagger_{i\sigma} d_{i\sigma} - 1)^2 = \left(\frac{\hat{N}+\hat{E}}{2} - 1\right)^2 + \left(\frac{\hat{N}-\hat{E}}{2} - 1\right)^2 = \frac{\left(\hat{N}-2\right)^2 - \hat{E}^2}{2},$$

with $\hat{N} = \sum_\sigma \hat{N}_\sigma$, $\hat{E} = \sum_\sigma \hat{E}_\sigma$. Note that opeator $\hat{N}$ represents the total occupation number inside both dots. If this occupation is different than 2 there is an imbalance between particles and dots that is punished by this term. The term E^2 is much more interesting since this one is the responsible for the emergence of satellite peaks in the DOS. To understand what it makes it is simple to observe its results when applied to a based ordered by $|+,-\rangle$.

$$\hat{E}^2|\uparrow,0\rangle = \hat{E}|0,\uparrow\rangle = |\uparrow,0\rangle$$

$$\hat{E}^2|\uparrow,\downarrow\rangle = \hat{E}\left(|0,\uparrow\downarrow\rangle + |\uparrow\downarrow,0\rangle\right) = 2|\uparrow,\downarrow\rangle - 2|\downarrow,\uparrow\rangle$$

The new Hamiltonian

$$H = \sum_\sigma \frac{U}{4}\left(\left(\hat{N}-2\right)^2 - \hat{E}^2\right) + \frac{t}{\sqrt{2}}(d_{+,\downarrow} + d^\dagger_{+,\downarrow})\gamma_1 + \frac{\Gamma}{\sqrt{2}}\sum_k (d^\dagger_{+,\sigma} c_{k\sigma} + c^\dagger_{k\sigma} d_{+,\sigma}) \tag{B.2}$$

is represented in **??**

We can explain this three-peak as the result of a new strong coupling interaction characterized by the spin exchange between both dots.

In addition, the spin-up DOS at the Fermi energy grows faster than the spin-down DOS, breaking the initial spin-symmetry when $t_1 = t_2 = 0$. At $t_1 = t_2 = 0.02D$ the spin-up DOS at the fermi energy doubles the spin-down DOS which implies that the Majorana signature is present in both dots. Indeed **??** shows that the relation $\frac{\rho_\uparrow(0)}{\rho_\uparrow(0)}$ increases continuously from 1 to 2. Note that the Majorana is completely attached when the coupling t_1 reaches the order of $0.01D$.

B.1 Initial DQD-Majorana Hamiltonian.

$H_{N_\uparrow=0,P_\downarrow=-1}$:

$$\begin{array}{c} |\downarrow,\downarrow,\downarrow\rangle \rightarrow \\ |0,0,\downarrow\rangle \rightarrow \\ |0,\downarrow,0\rangle \rightarrow \\ |\downarrow,0,0\rangle \rightarrow \end{array} \begin{bmatrix} \varepsilon_d^+ + \frac{U^+}{2} - 2h + \varepsilon_m & 0 & -\tilde{t}_{+1} & \tilde{t}_{+2} \\ 0 & \frac{U^+}{2} + \varepsilon_m & \tilde{t}^*_{-2} & \tilde{t}^*_{-1} \\ -\tilde{t}^*_{+1} & \tilde{t}_{-2} & \varepsilon_{d_2} + \frac{U^+}{2} - h - \varepsilon_m & t \\ \tilde{t}^*_{+2} & \tilde{t}_{-1} & t^* & \varepsilon_{d_1} + \frac{U^+}{2} - h - \varepsilon_m \end{bmatrix}$$

$H_{N_\uparrow=0,P_\downarrow=1}$:

$$\begin{array}{c} |0,0,0\rangle \rightarrow \\ |\downarrow,\downarrow,0\rangle \rightarrow \\ |\downarrow,0,\downarrow\rangle \rightarrow \\ |0,\downarrow,\downarrow\rangle \rightarrow \end{array} \begin{bmatrix} \frac{U^+}{2}-\varepsilon_m & 0 & \tilde{t}_{+1} & \tilde{t}_{+2} \\ 0 & \varepsilon_d^+ + \frac{U^+}{2} - 2h - \varepsilon_m & \tilde{t}^*_{-2} & -\tilde{t}^*_{-1} \\ \tilde{t}^*_{+1} & \tilde{t}_{-2} & \varepsilon_{d_1} + \frac{U^+}{2} - h + \varepsilon_m & t \\ \tilde{t}^*_{+2} & -\tilde{t}_{-1} & t^* & \varepsilon_{d_2} + \frac{U^+}{2} - h + \varepsilon_m \end{bmatrix}$$

$H_{N_\uparrow=2,P_\downarrow=-1}$:

$$\begin{array}{c} |\uparrow\downarrow,\uparrow\downarrow,\downarrow\rangle \rightarrow \\ |\uparrow,\uparrow,\downarrow\rangle \rightarrow \\ |\uparrow,\uparrow\downarrow,0\rangle \rightarrow \\ |\uparrow\downarrow,\uparrow,0\rangle \rightarrow \end{array} \begin{bmatrix} 2\varepsilon_d^+ + \frac{3U^+}{2} + \varepsilon_m & 0 & \tilde{t}_{+1} & \tilde{t}_{+2} \\ 0 & \varepsilon_d^+ + \frac{U^+}{2} + 2h + \varepsilon_m & \tilde{t}^*_{-2} & -\tilde{t}^*_{-1} \\ \tilde{t}^*_{+1} & \tilde{t}_{-2} & f(d_1,d_2) + h - \varepsilon_m & -t \\ \tilde{t}^*_{+2} & -\tilde{t}_{-1} & -t^* & f(d_2,d_1) + h - \varepsilon_m \end{bmatrix}$$

with $f(d_i,d_j) = \varepsilon_{d_i} + \frac{U_i}{2} + 2\varepsilon_{d_j} + \frac{3U_j}{2}$.
$H_{N_\uparrow=2,P_\downarrow=1}$:

$$\begin{array}{c} |\uparrow,\uparrow,0\rangle \rightarrow \\ |\uparrow\downarrow,\uparrow\downarrow,0\rangle \rightarrow \\ |\uparrow\downarrow,\uparrow,\downarrow\rangle \rightarrow \\ |\uparrow,\uparrow\downarrow,\downarrow\rangle \rightarrow \end{array} \begin{bmatrix} \varepsilon_d^+ + \frac{U^+}{2} + 2h - \varepsilon_m & 0 & -\tilde{t}_{+1} & \tilde{t}_{+2} \\ 0 & 2\varepsilon_d^+ + \frac{3U^+}{2} - \varepsilon_m & \tilde{t}^*_{-2} & \tilde{t}^*_{-1} \\ -\tilde{t}^*_{+1} & \tilde{t}_{-2} & f(d_2,d_1) + h + \varepsilon_m & -t \\ \tilde{t}^*_{+2} & \tilde{t}_{-1} & -t^* & f(d_1,d_2) + h + \varepsilon_m \end{bmatrix}$$